Supplementary Information

Table of Contents

Materials and Methods

Materials:

All the chemicals and solvents were purchased from *J&K* Scientific Ltd. and Sigma-Aldrich and used without further purification. The cellulose paper was purchased from Titan Co. Ltd.

Characterization methods:

^{1}H NMR and ^{13}C NMR spectra were collected on a Q. One Instruments Quantum-I 400 M, and tetramethyl silane was used as the internal standard. High-resolution mass spectrometry (HRMS) analyses were conducted on a Bruker FTMS. Single crystal X-ray diffraction (XRD) was performed on Bruker Smart APEXII CCD diffractometer using graphite monochromate Cu Kα radiation. UV-Vis-NIR absorption spectra were measured on an Agilent Technologies spectrophotometer (Cary Series UV-Vis-NIR Spectrophotometer). Photoluminescence spectroscopy spectra were recorded on the Edinburgh FSL1000 spectrophotometer. Element analyses were performed using a vario EL Cube element analyzer. Scanning electron microscopy (SEM) was carried out with a Thermometer Scientific phenmo prox.

Cyclic voltammetry was performed on a CHI660E electrochemical workstation at a scanning rate of 0.1 V/s with an N_2 saturated solution of 0.1 M tetrabutylammonium hexafluorophosphate (Bu_4NPF_6) in CH_2Cl_2. A glassy carbon electrode was used as the working electrode, Ag/Ag^+ was used as the reference electrode, and platinum wire was used as the counting electrode. Fc^+/Fc (0.1 M in DCM) as the reference.

Electron paramagnetic resonance (EPR) spectra were recorded with a Bruker ELEXSYS-II E500 spectrometer (X-band, MW frequency 9.8431~9.8480 GHz, MW power of 0.20 mW, modulation frequency of 100 kHz, and modulation amplitude of 0.50 mT) equipped with a high-Q cylindrical resonator ER4119HS.

Theoretical calculation. Kohn-Sham density functional theory (DFT), as implemented in the Gaussian (G16) package, was used for all computations, employing the PBE0 functional and the def2-SV(P) basis. For neutral and oxidized species, solvent effects were considered by means of the polarizable continuum model (PCM) for dichloromethane and acetonitrile, respectively, to match the experimental conditions. “D3” dispersion corrections were included in the calculations.

Photothermal characterization measurements. The sunlight was generated through a solar simulator for the standard AM 1.5 G spectrum (CEL-S500/350/150). The temperature response of the sample was measured with an IR thermal camera (FLIR T630sc).

Solar steam generation experiments. The $\mathbf{2}^{\bullet+}SbF_6^-$ cellulose paper was surrounded by polystyrene foam to reduce heat loss. The sunlight was generated through a solar simulator for the standard AM 1.5 G spectrum (CEL-S500/350/150). The weight loss of water was measured by an electronic mass balance, and the temperature over the process was recorded by an IR thermal camera.

Desalination of seawater. By adding appropriate amounts of sodium chloride, magnesium chloride, calcium chloride, and potassium chloride to deionized water, seawater was obtained. The concentrations of all the five primary ions (Na^+, Mg^{2+}, $Ca^{2+,}$ and K^+) were examined by inductively coupled plasma spectroscopy (ICP-OES, Arcos II MV) before and after desalination.

Calculation of the efficiency for solar to vapor generation:

The conversion efficiency η of solar energy in photothermal-assisted water evaporation was calculated as the following formula[1-3]:

$$\eta = \frac{\Delta m h_{LV}}{E_{in}} \times 100\%$$

where Δm refers to the mass flux (evaporation rate) of water, h_{LV} refers to the total liquid-vapor phase-change enthalpy (i.e., the sensible heat and the enthalpy of vaporization, $h_{LV} = Q + \Delta h_{vap}$), Q is the energy provided to heat the system from the initial temperature T_0 to a final temperature T, Δh_{vap} is the latent heat of vaporization of water, and E_{in} is the energy input of light illumination (1 Sunlight = 3600 kJ·m^{-2}·h^{-1}). The schematic for the vaporization enthalpy of the vapor was as follows:

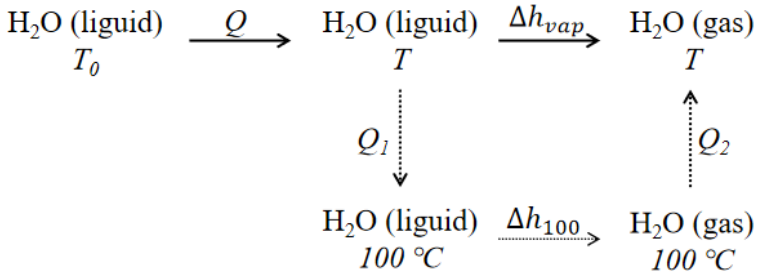

$Q = C_{liquid} \times (T\text{-}T_0)$

$\Delta h_{vap} = Q_1 + \Delta h_{100} + Q_2$

$Q_1 = C_{liquid} \times (100\text{-}T_0)$

$Q_2 = C_{vapor} \times (T\text{-}100)$

In this work, C_{liquid}, the specific heat capacity of liquid water is a constant of 4.18 J·g^{-1}·℃$^{-1}$. C_{vapor}, the specific heat capacity of water vaper is a constant of 1.865 J·g^{-1}·℃$^{-1}$. Δh_{100} is the latent heat of vaporization of water at 100 ℃, taken to be 2260 kJ·kg^{-1}. Thus, the surface temperature of **2**$^{\bullet+}$$SbF_6^-$ cellulose paper was 44.0 ℃ during the evaporation process, therefore T is 44.0 ℃. As the above formulas:

$Q = C_{liquid} \times (T\text{-}T_0) = 4.18 \times (44\text{-}25) = 81.51$ kJ·kg^{-1}

$\Delta h_{vap} = Q_1 + \Delta h_{100} + Q_2 = 4.18 \times (100\text{-}44) + 2260 + 1.865 \times (44\text{-}100) = 2389.64$ kJ·kg^{-1}

$h_{LV} = Q + \Delta h_{vap} = 81.51 + 2389.64 = 2471.15$ kJ·kg^{-1}

$\Delta m = 1.60$ kg·m^{-2}·h^{-1}

$$\eta = \frac{\Delta m h_{LV}}{E_{in}} \times 100\% = \frac{1.602 \times 2471.15}{3600} \times 100\% = 110\%$$

As a result, evaporation efficiency η = 110% when the latent heat of water vaporization at 44.0 ℃ (2471.15 kJ·kg^{-1}) is used in the calculation.

Synthesis and Characterization

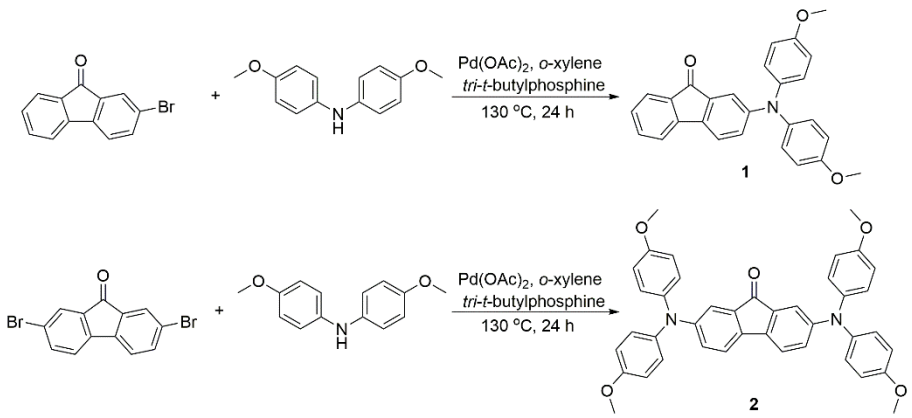

Figure S1. Synthetic routes for **1** and **2**.

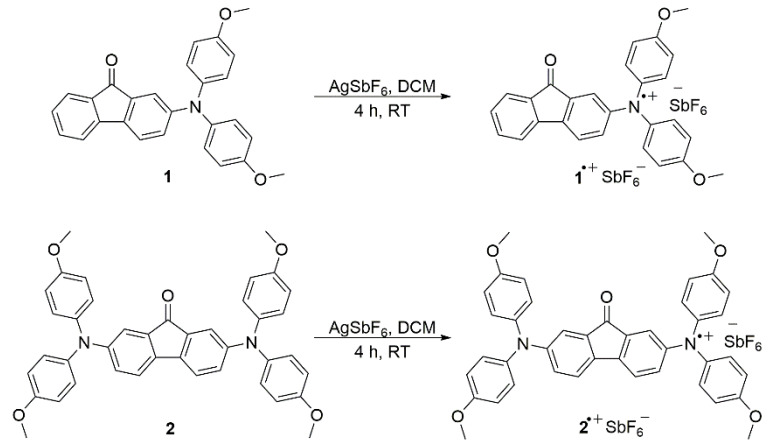

Figure S2. Synthetic routes for $\mathbf{1}^{\bullet+}SbF_6^-$ and $\mathbf{2}^{\bullet+}SbF_6^-$.

Synthesis of 1

A solution of 2-bromo-9-fluorenone (6 mmol), 4,4′ -dimethoxy diphenylamine (6 mmol), and sodium *t*-butoxide (7.2 mmol) in dry *o*-xylene (40 mL) was stirred under nitrogen for 30 min. Palladium (II) acetate (Pd $(OAc)_2$) (0.12 mmol) and tri-*t*-butyl phosphine (0.12 mmol) in dry *o*-xylene (40 mL) were added to the solution as a catalyst. The solution was heated under reflux at about 130 °C in a nitrogen atmosphere for 24 h. After cooling, the solution was evaporated to remove *o*-xylene, and chloroform (150 mL) was added. The organic phase was washed with H_2O, dried over Na_2SO_4, and filtered. Evaporation of the filtrate gave the crude product, which was then purified by column chromatography (silica gel; eluent: ethyl acetate: hexane = 1: 5) to yield **1** as a deep red powder (3.9 mmol, 65%). ^1H NMR (400 MHz, DMSO-d_6), δ (ppm): 7.60-7.58 (d, J = 8.0 Hz, 1H), 7.54-7.49 (m, 3H), 7.25-7.21 (t, J = 8.0 Hz, 1H), 7.13-7.09 (m, 4H), 6.98-6.94 (m, 4H), 6.88-6.83 (m, 2H), 3.76 (s, 6H). ^{13}C NMR (100 MHz, DMSO-d_6), δ (ppm) = 194.29, 156.48, 150.25, 145.26, 140.25, 135.63, 135.60, 134.92, 134.42, 127.62, 127.06, 124.70, 124.36, 121.04, 119.45, 116.04, 115.06, 55.64. HRMS (ESI) *m*/*z* calcd. for $C_{27}H_{22}NO_3$ $[M+H]^+$: 408.1594; found: 408.1587.

Synthesis of 2

A solution of 2,7-dibromo-9H-fluoren-9-one (6 mmol), 4,4′ -dimethoxy diphenylamine (12 mmol),

and sodium *t*-butoxide (12 mmol) in dry *o*-xylene (50 mL) was stirred under nitrogen for 30 min. Palladium (II) acetate (Pd $(OAc)_2$) (0.24 mmol) and tri-*t*-butyl phosphine (0.24 mmol) in dry *o*-xylene (50 mL) were added to the solution as a catalyst. The solution was heated under reflux at about 130 °C in a nitrogen atmosphere for 24 h. After cooling, the solution was evaporated to remove *o*-xylene, and chloroform (200 mL) was added. The organic phase was washed with H_2O, dried over Na_2SO_4, and filtered. Evaporation of the filtrate gave the crude product, which was then purified by column chromatography (silica gel; eluent: ethyl acetate: hexane = 1: 8) to yield **2** as a deep green powder (3 mmol, 50%). ^{1}H NMR (400 MHz, DMSO-d_6), δ (ppm): 7.34-7.32 (d, J = 8.0 Hz, 2H), 7.07-7.03 (m, 8H), 6.95-6.92 (m, 8H), 6.84-6.81 (m, 2H), 6.78-6.77 (d, J = 4.0 Hz, 2H), 3.74 (s, 12H). ^{13}C NMR (100 MHz, DMSO-d_6), δ (ppm) = 193.21, 156.16, 148.58, 139.40, 135.51, 134.60, 127.07, 124.03, 120.85, 115.10, 113.8955.24. HRMS (ESI) *m/z* calcd. for $C_{41}H_{35}N_2O_5$ $[M+H]^+$: 635.2540; found: 635.2537.

Synthesis of $1^{\bullet+}SbF_6^-$

Under anaerobic and anhydrous conditions, a mixture of **1** (40 mg, 0.1 mmol) and $AgSbF_6$ (34 mg, 0.1 mmol) in CH_2Cl_2 (20 mL) was stirred at room temperature for 4 h. The resultant black-red solution was filtered to remove the gray precipitate (Ag metal). The filtrate was then concentrated to yield radical cation $\mathbf{1}^{\bullet+}SbF_6^-$ as a black-red powder. Yield: 58 mg, 90%. Elemental analysis calcd (%) for $C_{27}H_{21}F_6NO_3Sb$: C 50.38, H 3.30, N 2.18; Found: C 49.36, H 3.32, N 2.67.

Synthesis of $2^{\bullet+}SbF_6^-$

Under anaerobic and anhydrous conditions, a mixture of **2** (63 mg, 0.1 mmol) and $AgSbF_6$ (34 mg, 0.1 mmol) in CH_2Cl_2 (20 mL) was stirred at room temperature for 4 h. The resultant black-green solution was filtered to remove the gray precipitate (Ag metal). The filtrate was then concentrated to yield radical cation $\mathbf{2}^{\bullet+}SbF_6^-$ as a black-green powder. Yield: 75 mg, 86%. Elemental analysis calcd (%) for $C_{41}H_{34}F_6N_2O_5Sb$: C 56.55, H 3.94, N 3.23; Found: C 55.50, H 3.96, N 3.36.

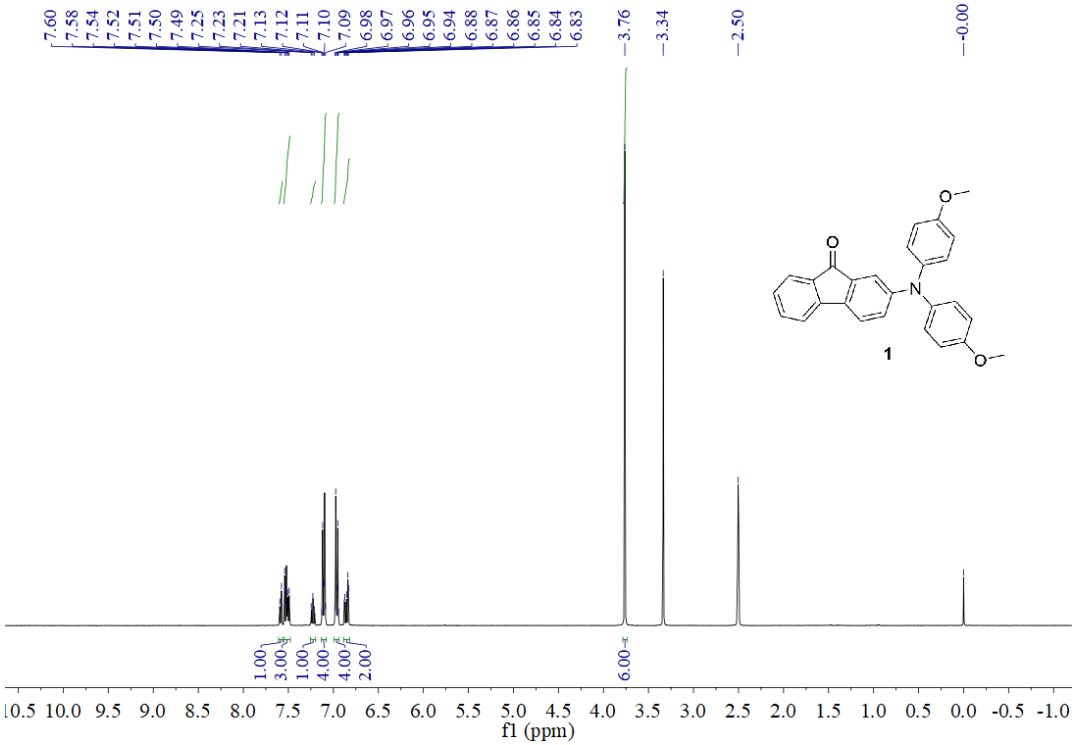

Figure S3. ^{1}H NMR spectrum of **1** in DMSO-d_6.

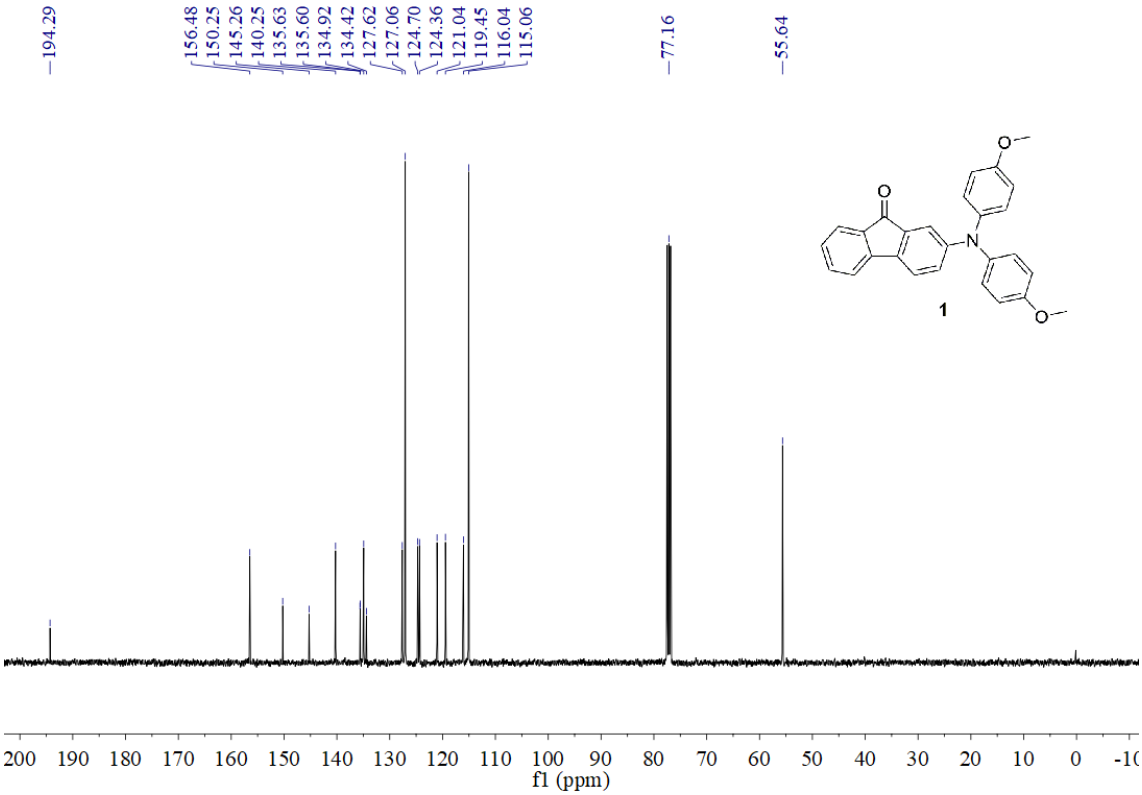

Figure S4. ^{13}C NMR spectrum of **1** in $CDCl_3$.

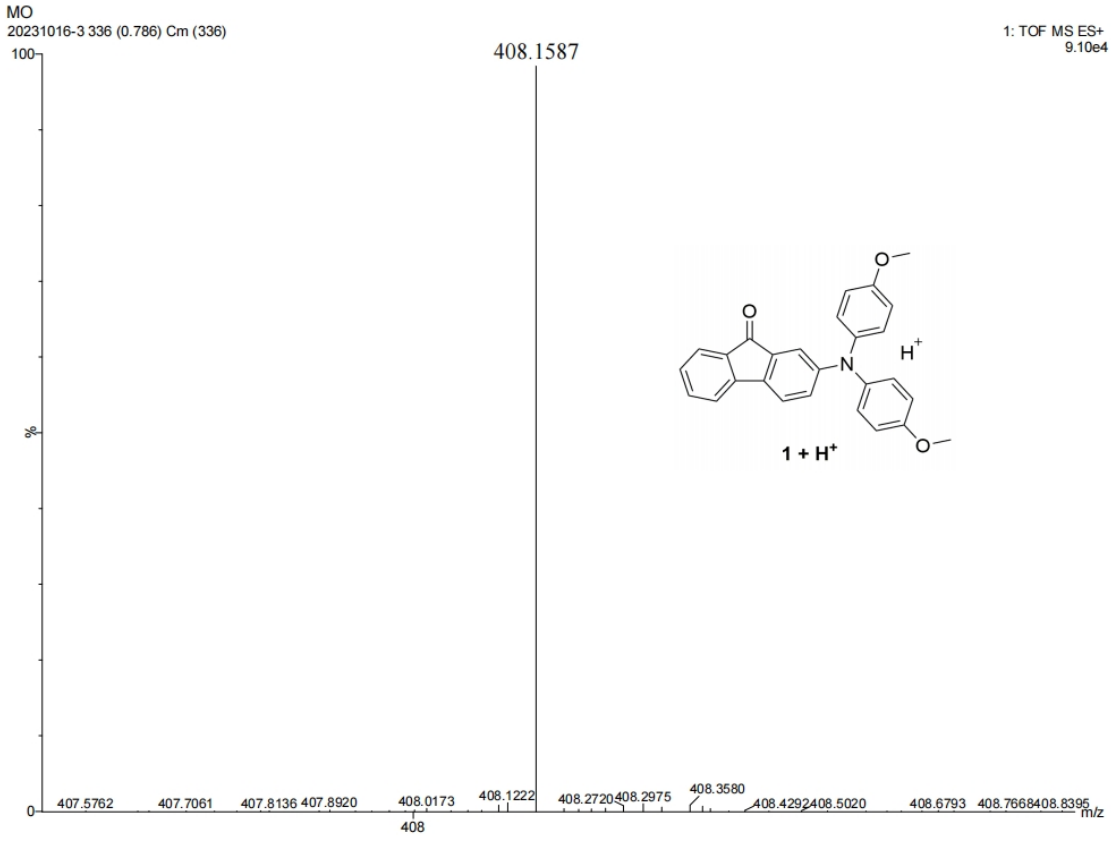

Figure S5. HRMS spectrum of **1**.

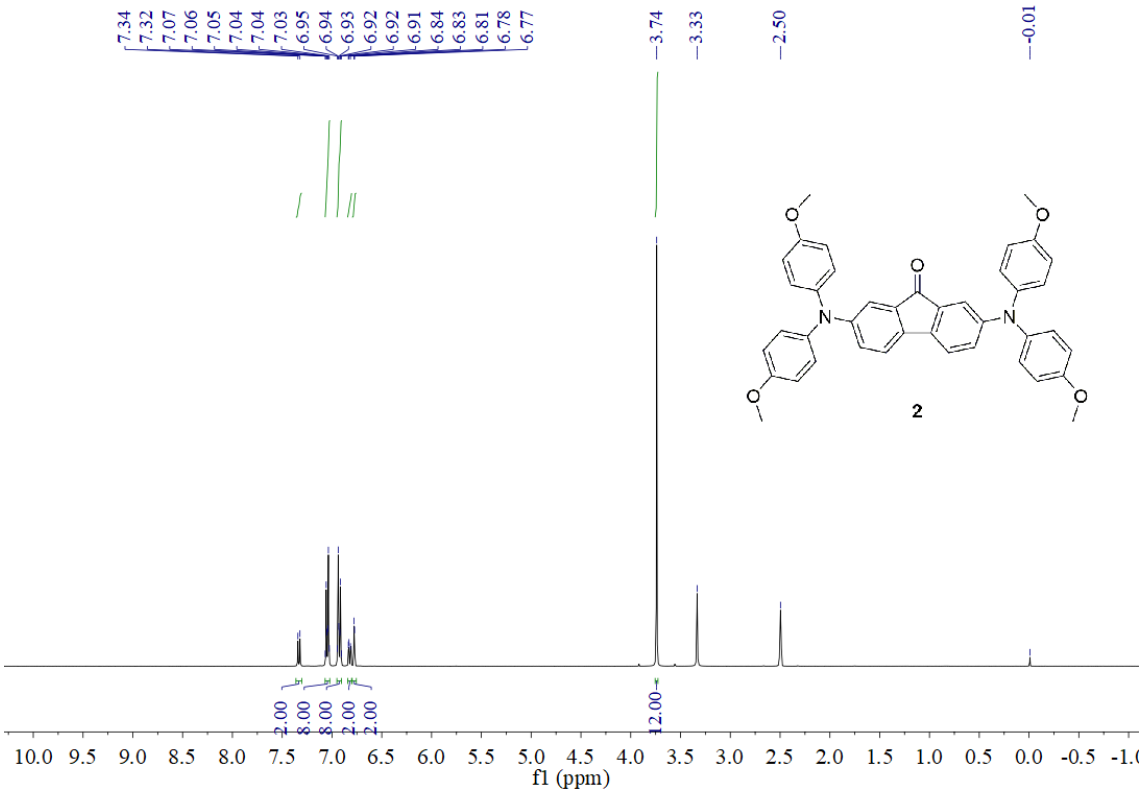

Figure S6. ^{1}H NMR spectrum of **2** in DMSO-d_6.

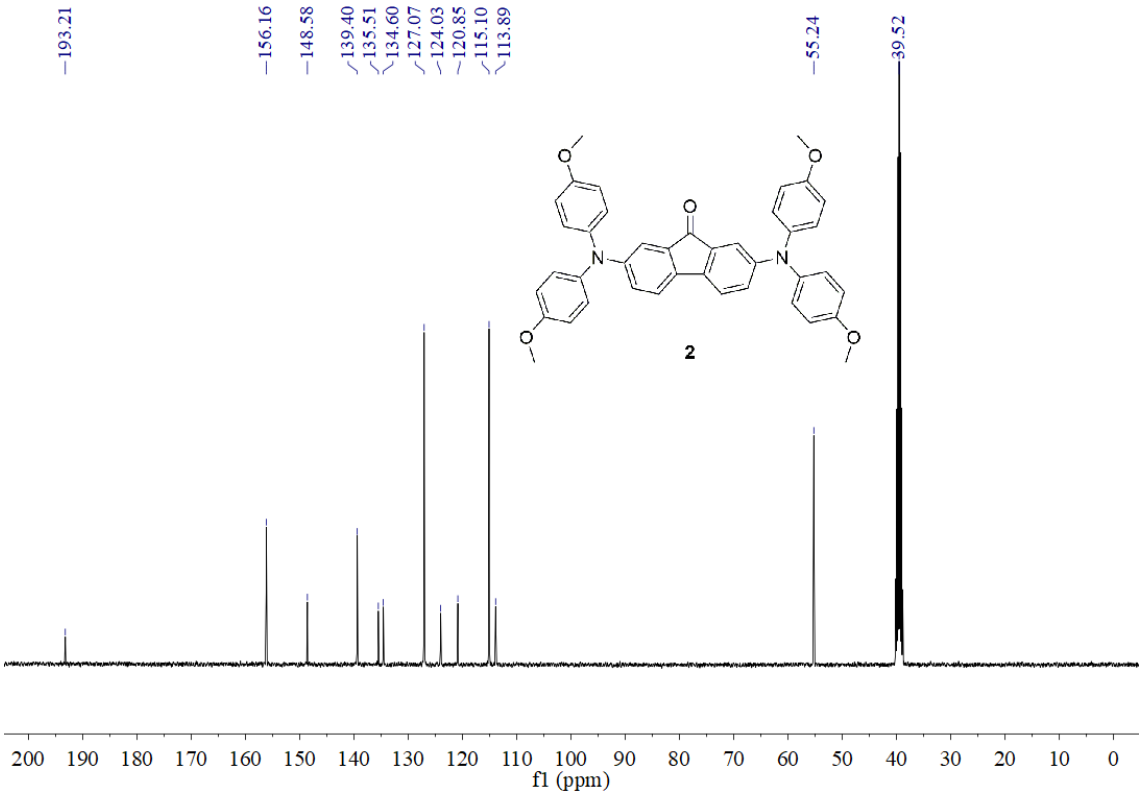

Figure S7. ^{13}C NMR spectrum of **2** in DMSO-d_6.

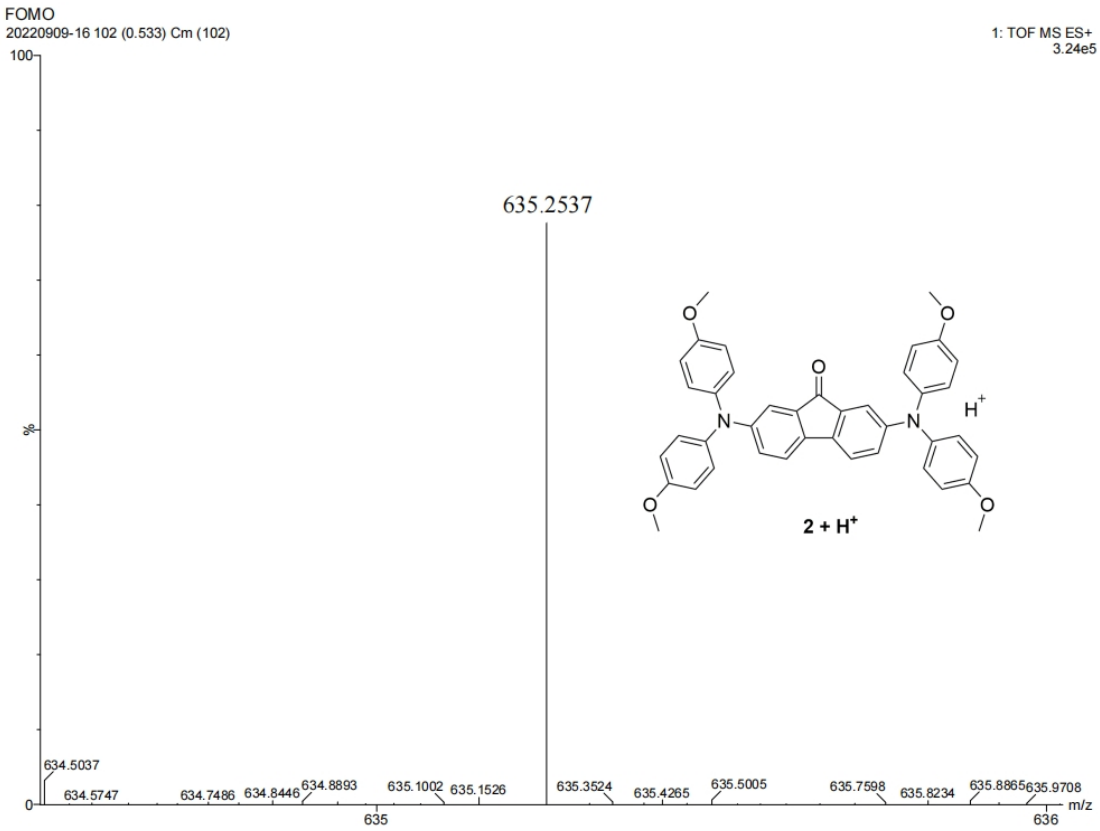

Figure S8. HRMS spectrum of **2**.

Radical cations $1^{\bullet+}SbF_6^-$ and $2^{\bullet+}SbF_6^-$

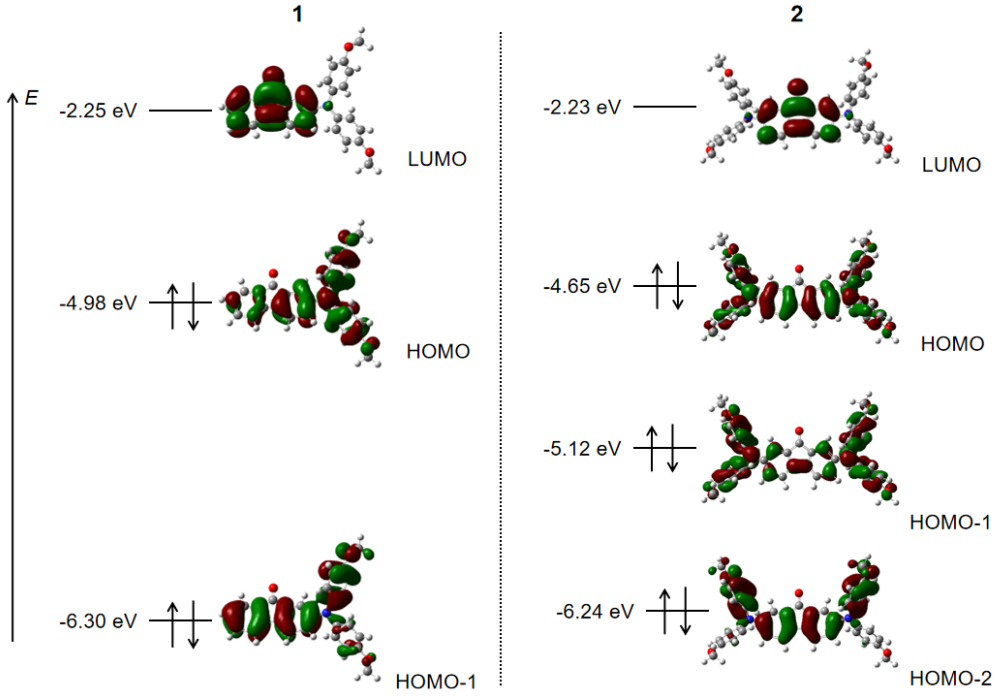

Figure S9. The frontier molecular orbitals and corresponding HOMO and LUMO energies of **1** and **2** were calculated using the B3LYP/6-31G* basis set.

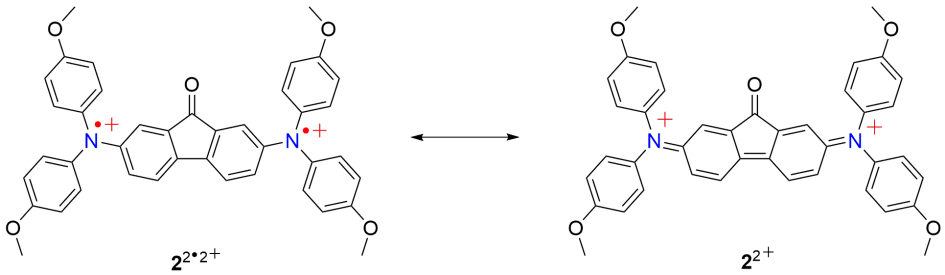

Scheme S1. Resonance structures of $\mathbf{2}^{2+}$.

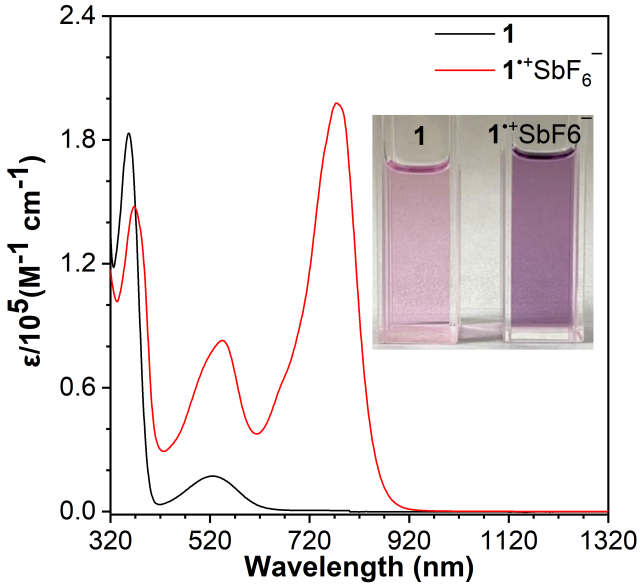

Figure S10. The UV–Vis-NIR absorption spectra of **1** and $\mathbf{1}^{\bullet+}SbF_6^-$ in CH_2Cl_2 (10^{-4} M). The inset shows the photos of **1** and $\mathbf{1}^{\bullet+}SbF_6^-$ in CH_2Cl_2 taken under daylight.

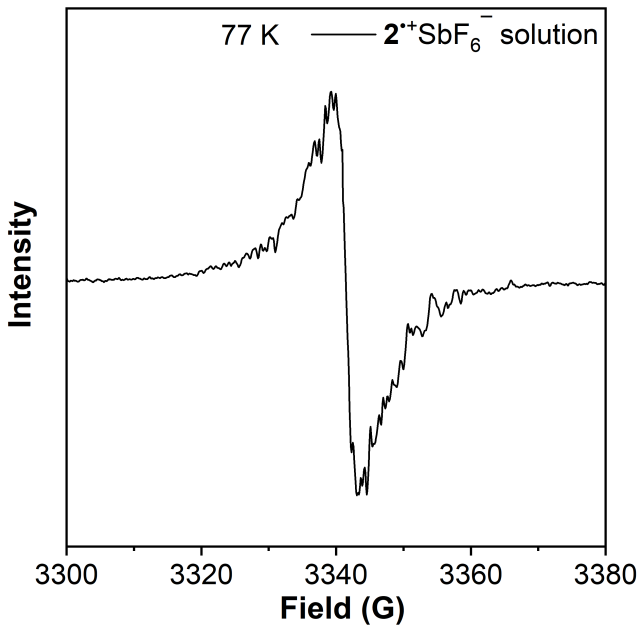

Figure S11. EPR spectra of $\mathbf{2}^{\bullet+}SbF_6^-$ in CH_2Cl_2 (10^{-4} M) at 77 K.

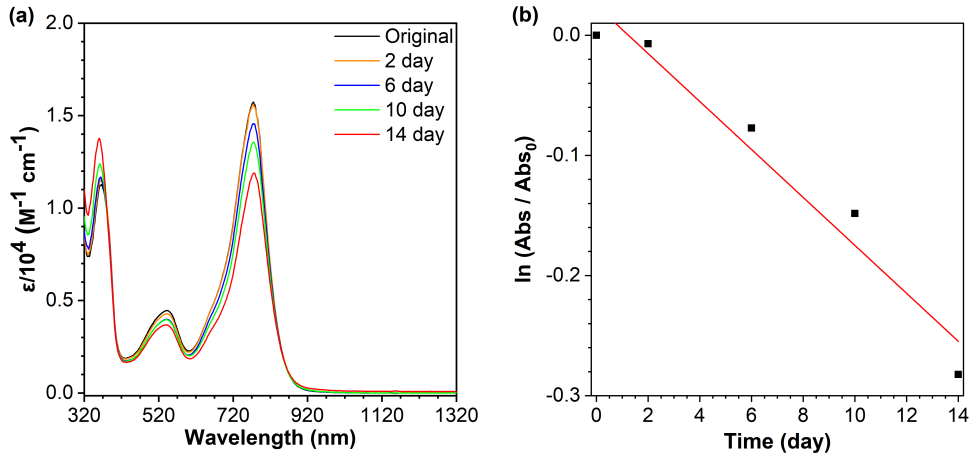

Figure S12. (a) In an air atmosphere, the absorption spectrum of $\mathbf{1}^{\bullet+}SbF_6^-$ changes over time in CH_2Cl_2 (10^{-4} M). (b) The first-order fitting plot of the absorption of $\mathbf{1}^{\bullet+}SbF_6^-$ at 775 nm over time under an air atmosphere.

Table S1. Linear fitting of the first-order fitting equation and calculation of the half-life.

Environment	A	B	r^2	Half-life (days)
Air	0.02471	-0.01995	0.96	35

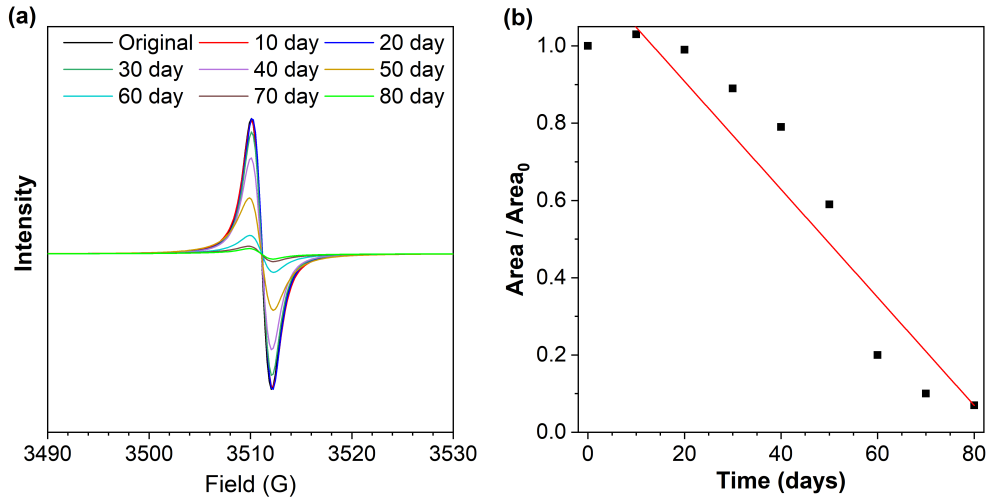

Figure S13. (a) Decay plot of $\mathbf{1}^{\bullet+}SbF_6^-$ powder monitored by EPR under air atmosphere. (b) The zero-order fitting plot of the concentration of radical cations as a function of time under air atmosphere.

Table S2. Linear fitting of the zero-order fitting equation and calculation of the half-life.

Environment	A	B	r^2	Half-life (days)
Air	1.19	-0.014	0.91	49

Table S3. The Marcus reorganization energy λ, electronic coupling parameter H_{ab}, and additional relevant parameters of $\mathbf{2}^{\bullet+}SbF_6^-$.

v_{max} (cm^{-1})	5971
λ (cm^{-1})	5971
$v_{\frac{1}{2}}$ (cm^{-1})	3000
ε_{max} (cm^{-1})	11000
r_{AB} (Å)	9.7
H_{ab} (cm^{-1})	1200

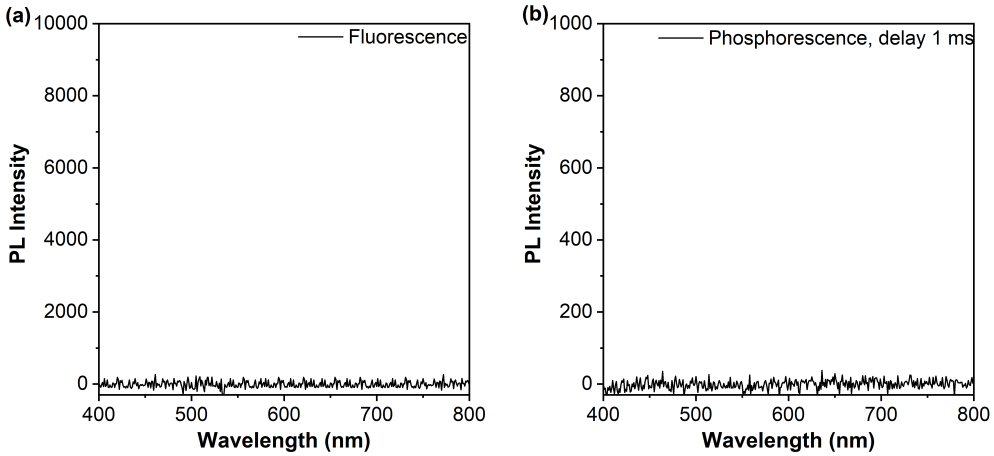

Figure S14. The fluorescence and phosphorescence spectra of $\mathbf{2}^{\bullet+}SbF_6^-$ in the solid state at room temperature (λ_{ex} = 380 nm).

Photothermal conversion of $\mathbf{2}^{\bullet+}SbF_6^-$

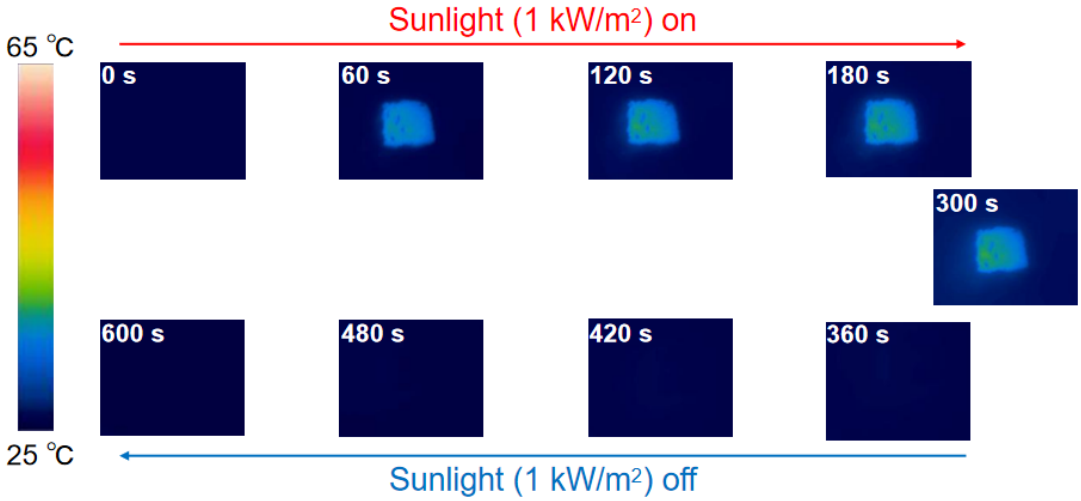

Figure S15. Infrared thermal images of **2** under 1 Sunlight irradiation and after turning off the light.

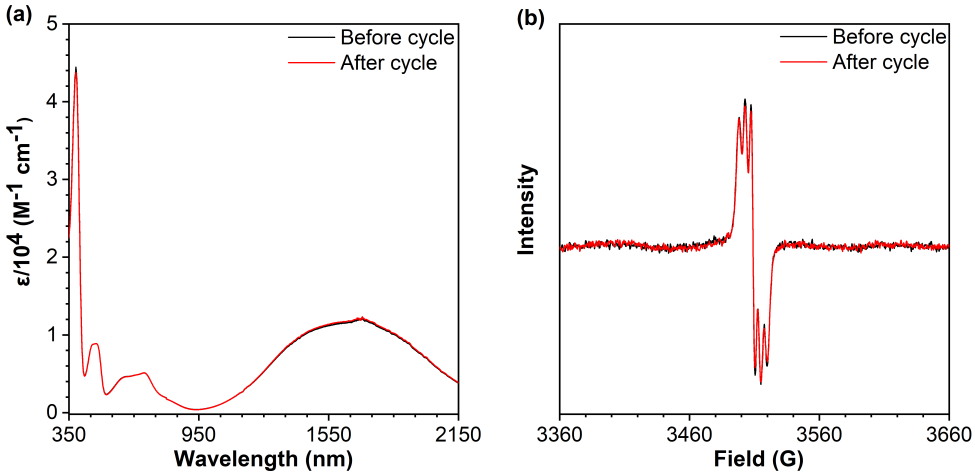

Figure S16. The UV-Vis-NIR absorption spectra (10^{-4} M) and solution EPR spectra (10^{-4} M) of $\mathbf{2}^{\bullet+}SbF_6^-$ before and after the photothermal cycle.

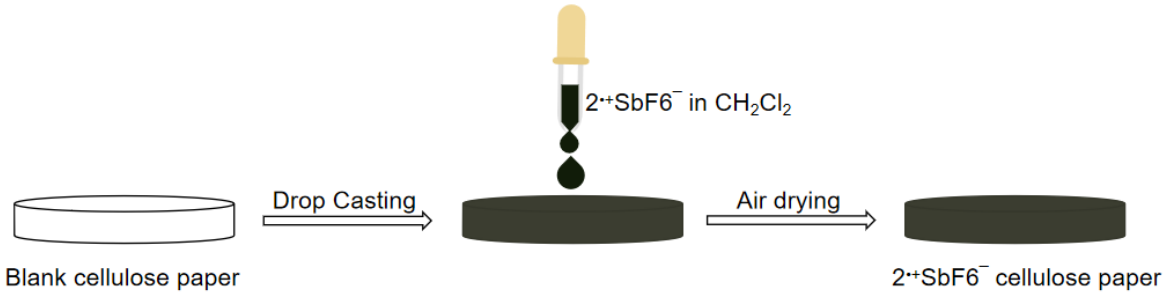

Figure S17. Schematic illustration of the drop-casting method for preparing $\mathbf{2}^{\bullet+}SbF_6^-$ cellulose paper.

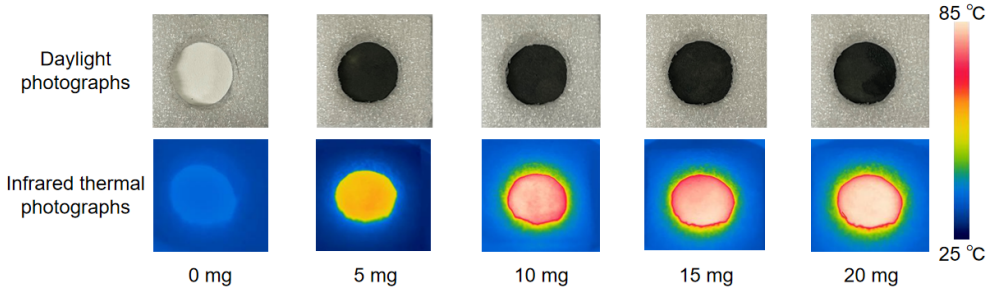

Figure S18. Under 1 Sunlight irradiation (1 kW·m^{-2}), daylight photographs and infrared thermal photographs of cellulose paper loaded with $\mathbf{2}^{\bullet+}SbF_6^-$ (0 mg, 5 mg, 10 mg, 15 mg, 20 mg).

Table S4. Performance metrics of some reported materials for solar-driven water evaporation.

System	Mass change (kg·m^{-2}·h^{-1})	Solar-to-vapor efficiency (%)	Reference
$\mathbf{2}^{\bullet+}SbF_6^-$ cellulose paper	1.60	110	This work.
CR-TPE-T	1.272	87.2	*Adv. Mater.*, 2020, **32**, 1908537.
GDPA-QCN	1.3	90.4	*Angew. Chem. Int. Ed.*, 2022, **61**, e202117087.
DDPA-PDN	0.89	73.98	*Adv. Funct. Mater.*, 2021, **31**,

			2106247.
CTC	1.67	90.3	*ACS Energy Lett*, 2020, **5**, 2698−2705.
TPAD	1.42	94	*Angew. Chem. Int. Ed.*, 2022, **61**, e202201900.
IDT-O_4	1.365	94.38	*Aggregate.,* 2024, **5**, e426.
TPA-TPA-O_6	1.293	89.41	*Angew. Chem. Int. Ed.* 2022, **61**, e202113653.
GS-POP-2	1.402	96.8	*Angew. Chem. Int. Ed.* 2021, **60**, 24424 – 24429.
4OCSPC	1.262	86.6	*J. Mater. Chem. A,* 2021, **9**, 24452 – 24459.
GS-COF-1-3 d	1.38	95.3	*Sol. RRL,* 2021, **5**, 2100762
NKU-123	1.442	97.8	*Angew. Chem. Int. Ed.* 2024, **63**, e202401766.
PU-THAC	1.407	97	*Angew. Chem. Int. Ed.* 2022, **61**, e202202571.
2TP-BBT	1.35	94.3	*J. Mater. Chem. A,* 2023, **11**, 15380-15388.
ASP-F4TCNQ	1.80	87	*ChemSusChem,* 2023, **16**, e202300644.
E-T	2.1	86.9	*J. Mater. Chem. A*, 2023, **11**, 2933-2946.
OSB-F4TCNQ	2.0	88.9	*Angew. Chem. Int. Ed.* 2024, **63**, e202318628.

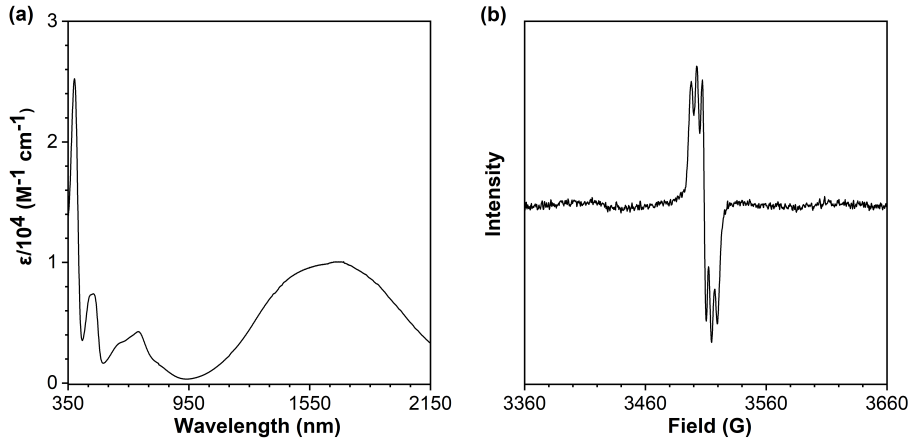

Figure S19. After undergoing three cycles, the $\mathbf{2}^{\bullet+}SbF_6^-$ cellulose paper was dissolved in CH_2Cl_2, and the UV-Vis-NIR absorption spectrum (≈10^{-4} M) and EPR spectrum (≈10^{-4} M) were measured.

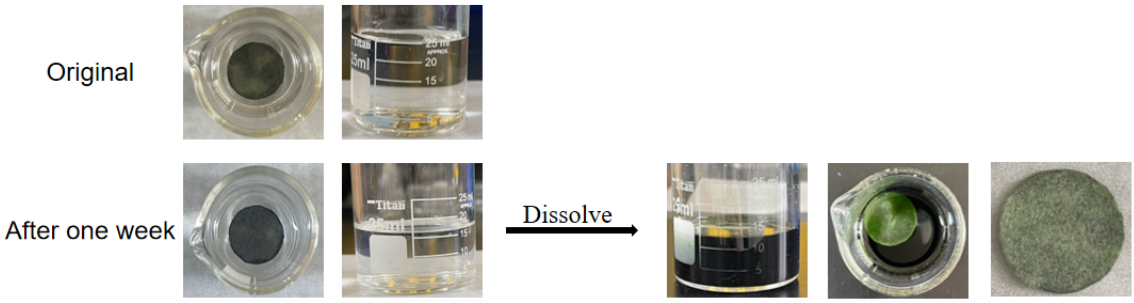

Figure S20. The stability of $\mathbf{2}^{\bullet+}SbF_6^-$ cellulose paper after soaking in water for one week.

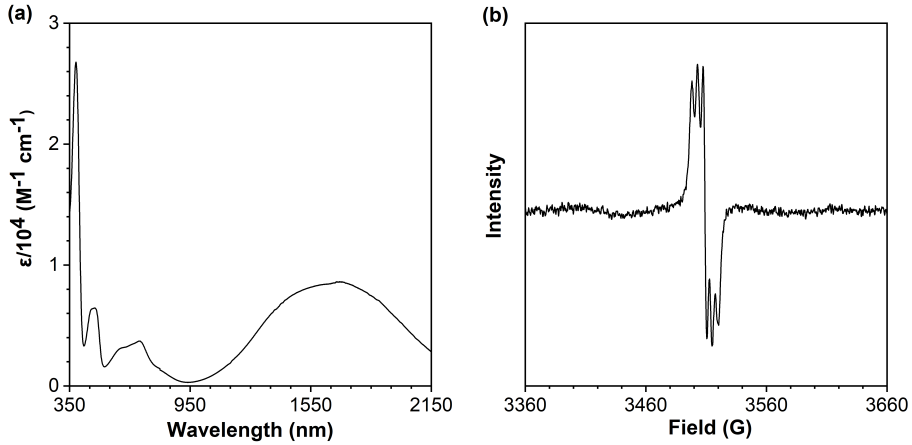

Figure S21. After soaking in water for one week, the $\mathbf{2}^{\bullet+}SbF_6^-$ cellulose paper was redissolved in CH_2Cl_2, and the UV-Vis-NIR absorption spectrum (≈10^{-4} M) and EPR spectrum (≈10^{-4} M) were measured.

Single Crystal Data

Table S5. Crystal data and structure refinement for **1**.

Empirical formula	C27 H21 N O3
Formula weight	448.50
Temperature	150(2) K
Wavelength	1.54178 Å
Crystal system	orthorhombic
Space group	P b c a
Unit cell dimensions	a = 20.4300(4) Å alpha = 90 deg. b = 8.0475(2) Å beta = 90 deg. c = 28.4110(6) Å gamma = 90 deg.
Volume	4671.07(18) $Å^3$
Z	8
Density (calculated)	1.276 Mg/m^3
Absorption coefficient	0.665 mm^{-1}
F (000) Crystal size	1888.0 0.2 × 0.15× 0.1 cm^3
Theta range for data collection	3.790 to 74.695
Index ranges	-25<=h<=18, -9<=k<=10, -35<=l<=35
Reflections collected	30759
Independent reflections	4758 [R(int) = 0.0374]
Absorption correction	Spherical harmonics
Refinement method	SHELXL-2018/3 (Sheldrick, 2018)
Data / restraints / parameters	4758 / 0 / 310
Goodness-of-fit on F2	1.109
Final R indices [I>2sigma(I)]	R1 = 0.0693, wR2 = 0.2307
R indices (all data)	R1 = 0.0756, wR2 = 0.2307
Largest diff. peak and hole	0.612 and -0.233 $e.Å^{-3}$
CCDC reference	2356955

Table S6. Crystal data and structure refinement for **2**.

Empirical formula	C41 H34 N2 O5
Formula weight	634.70
Temperature	293 K
Wavelength	1.54184 Å
Crystal system	monoclinic
Space group	C c
Unit cell dimensions	a = 18.8192(4) Å alpha = 90 deg. b = 20.0992(5) Å beta = 101.550(2) deg. c = 9.0529(2) Å gamma = 90 deg.
Volume	3354.93(13) $Å^3$
Z	4

Density (calculated)	1.257 Mg/m^3
Absorption coefficient	0.665 mm^{-1}
F (000) Crystal size	1336.0 0.2 × 0.15× 0.1 cm^3
Theta range for data collection	3.253 to 76.745
Index ranges	-23<=h<=23, -24<=k<=24, -7<=l<=11
Reflections collected	11476
Independent reflections	4439 [R(int) = 0.0264]
Absorption correction	Spherical harmonics
Refinement method	SHELXL-2017/1 (Sheldrick, 2017)
Data / restraints / parameters	4439 / 2 / 437
Goodness-of-fit on F2	1.039
Final R indices [I>2sigma(I)]	R1 = 0.0802, wR2 = 0.2341
R indices (all data)	R1 = 0.0816, wR2 = 0.2303
Largest diff. peak and hole	0.360 and -0.274 $e.Å^{-3}$
CCDC reference	2356954

Computational part

XYZ coordinates

(+)-**1**$^+$

C	-0.76580	1.49818	-0.85883
C	-0.27152	0.32539	-0.25358
C	-1.19160	-0.58800	0.30546
C	-2.53908	-0.29808	0.23394
C	-3.03276	0.87592	-0.36188
C	-2.13168	1.78110	-0.90963
H	-0.05477	2.19963	-1.29937
H	-0.85449	-1.50686	0.78940
H	-2.47370	2.70103	-1.39033
C	-4.90478	-0.30030	0.40551
C	-6.23770	-0.58205	0.65500
C	-7.20073	0.33938	0.22782
C	-6.81054	1.50812	-0.42992
C	-5.46119	1.79053	-0.67927
C	-4.50320	0.87587	-0.25712
H	-6.51224	-1.50458	1.17260
H	-8.26103	0.14712	0.40749
H	-7.57415	2.21845	-0.75748
H	-5.17586	2.71088	-1.19446
C	-3.69173	-1.10370	0.75209
O	-3.64895	-2.16744	1.32243
N	1.10150	0.07012	-0.20746

C	2.03512	1.13052	-0.13255
C	3.16495	1.14239	-0.96526
C	1.86777	2.17549	0.77912
C	4.09413	2.16674	-0.88248
H	3.30945	0.32790	-1.67839
C	2.78678	3.22175	0.85289
H	0.99726	2.17399	1.43897
C	3.91381	3.22241	0.02307
H	4.97653	2.18261	-1.52514
H	2.61834	4.02191	1.57428
C	1.58817	-1.25867	-0.21728
C	2.58472	-1.65750	0.67569
C	1.09773	-2.19824	-1.13820
C	3.09100	-2.95664	0.65705
H	2.97693	-0.93430	1.39401
C	1.57954	-3.49687	-1.14769
H	0.32367	-1.89885	-1.84830
C	2.58501	-3.89153	-0.25286
H	3.87205	-3.22875	1.36755
H	1.19980	-4.23486	-1.85682
O	4.86574	4.17901	0.02277
O	2.99742	-5.17273	-0.34593
C	4.74381	5.25406	0.91037
H	5.61314	5.90280	0.74218
H	3.82399	5.83875	0.72743
H	4.74722	4.92224	1.96447
C	3.98645	-5.62991	0.53226
H	3.66685	-5.55774	1.58761
H	4.16189	-6.68564	0.28829
H	4.93484	-5.07543	0.41154

(+)-**2**$^{+}$

O	6.73480	5.02501	0.10239
O	8.50207	-4.29526	-0.07183
O	-0.01606	2.07031	1.13707
O	-6.87690	5.02118	0.33037
O	-8.59793	-4.23889	0.13366
N	4.78374	-0.16883	-0.19370
N	-4.85874	-0.13678	-0.09024
C	7.71541	5.41450	1.03680
H	8.65292	4.85015	0.89873
H	7.36229	5.28219	2.07323
H	7.90939	6.47892	0.85872
C	6.30693	3.75636	0.08983

C	6.76678	2.75377	0.95789
H	7.51686	2.96907	1.71876
C	6.25401	1.46501	0.86215
H	6.60665	0.68985	1.54559
C	5.28332	1.15071	-0.09466
C	4.83381	2.15293	-0.97106
H	4.09520	1.91071	-1.73817
C	5.33454	3.43828	-0.87527
H	4.99966	4.22404	-1.55483
C	8.32999	-5.45151	0.71517
H	7.42179	-6.00647	0.42565
H	8.27733	-5.20632	1.78919
H	9.20780	-6.08365	0.53578
C	7.56276	-3.34119	-0.05057
C	7.79804	-2.21982	-0.86676
H	8.71107	-2.19484	-1.46447
C	6.88508	-1.18273	-0.91714
H	7.06966	-0.31974	-1.56010
C	5.70984	-1.23772	-0.14986
C	5.48116	-2.34587	0.67257
H	4.58162	-2.38243	1.29084
C	6.39241	-3.39544	0.72180
H	6.18934	-4.24169	1.37797
C	3.42958	-0.40516	-0.32484
C	2.48477	0.51189	0.20562
H	2.80621	1.40580	0.74295
C	1.14975	0.23389	0.05186
C	-0.02615	1.02642	0.52932
C	-1.21760	0.24151	0.07857
C	-2.54699	0.52812	0.26124
H	-2.85149	1.42461	0.80414
C	-3.50886	-0.38339	-0.24776
C	-3.06359	-1.55016	-0.92139
H	-3.80708	-2.23535	-1.33139
C	-1.71589	-1.82290	-1.09569
H	-1.41168	-2.72226	-1.63476
C	-0.76934	-0.92209	-0.59451
C	0.67931	-0.92610	-0.61186
C	1.60892	-1.83066	-1.13761
H	1.28724	-2.72588	-1.67362
C	2.96176	-1.56668	-0.99257
H	3.69166	-2.25529	-1.42084
C	-6.46726	6.06931	-0.51830
H	-6.70249	5.85086	-1.57355

H	-5.38684	6.26884	-0.42188
H	-7.02504	6.95970	-0.20466
C	-6.34501	3.80312	0.17176
C	-5.38954	3.47457	-0.80212
H	-5.02895	4.22010	-1.51059
C	-4.90523	2.17392	-0.88606
H	-4.17926	1.91832	-1.66091
C	-5.34816	1.18653	0.00113
C	-6.30821	1.51697	0.97231
H	-6.65798	0.75141	1.66778
C	-6.79950	2.80641	1.05467
H	-7.53898	3.07920	1.80978
C	-8.41418	-5.39384	0.92017
H	-7.51580	-5.95441	0.61149
H	-9.29931	-6.02159	0.76275
H	-8.33567	-5.14578	1.99192
C	-7.65322	-3.29034	0.12987
C	-7.89988	-2.17128	-0.68622
H	-8.82572	-2.14343	-1.26371
C	-6.98195	-1.14021	-0.76177
H	-7.17515	-0.27936	-1.40505
C	-5.79031	-1.19908	-0.02039
C	-5.55017	-2.30471	0.80249
H	-4.63775	-2.34370	1.40143
C	-6.46645	-3.34811	0.87680
H	-6.25448	-4.19246	1.53255

Reference

1. Ginting, R. T.; Abdullah, H.; Barus, D. A.; Fauzia, V., Extremely high-efficiency solar steam generation, robust and scalable photothermal evaporator based on ZIF-67@MXene/rGO decorated rock wool. *J. Mater. Chem. A* **2023,** *11* (10), 5296-5308.
2. Xu, J.; Chen, Q.; Li, S.; Shen, J.; Keoingthong, P.; Zhang, L.; Yin, Z.; Cai, X.; Chen, Z.; Tan, W., Charge-Transfer Cocrystal via a Persistent Radical Cation Acceptor for Efficient Solar-Thermal Conversion. *Angew. Chem. Int. Ed.* **2022,** *61* (21), e202202571.
3. Su, Y.; Chen, Z.; Tang, X.; Xu, H.; Zhang, Y.; Gu, C., Design of Persistent and Stable Porous Radical Polymers by Electronic Isolation Strategy. *Angew. Chem. Int. Ed.* **2021,** *60* (46), 24424-24429.